Remote Sens. **2015**, *7*, 4858-4879; doi:10.3390/rs70404858

OPEN ACCESS

remote sensing

ISSN 2072-4292

www.mdpi.com/journal/remotesensing

Article

Hydrodynamic and Inundation Modeling of China's Largest Freshwater Lake Aided by Remote Sensing Data

Peng Zhang [1,2], Jianzhong Lu [2,*], Lian Feng [2], Xiaoling Chen [2,3,*], Li Zhang [3], Xiongwu Xiao [2] and Honggao Liu [1]

[1] Key Laboratory of Ecological Impacts of Hydraulic-Projects and Restoration of Aquatic Ecosystem of Ministry of Water Resources, The Institute of Hydroecology, Ministry of Water Resource and Chinese Academy of Sciences, Wuhan 430079, China; E-Mails: peterwin86@gmail.com (P.Z.); hugolaugene@gmail.com (H.L.)

[2] State Key Laboratory of Information Engineering in Surveying, Mapping and Remote Sensing, Wuhan University, Wuhan 430079, China; E-Mails: lianfeng619@gmail.com (L.F.); xiao_xiongwu@sina.com (X.X.)

[3] Key Laboratory of Poyang Lake Wetland and Watershed Research, Ministry of Education, Jiangxi Normal University, Nanchang 330022, China; E-Mail: zhanglinu@126.com

* Authors to whom correspondence should be addressed; E-Mails: lujzhong@whu.edu.cn (J.L.); xiaoling_chen@ whu.edu.cn (X.C.); Tel.: +86-27-6877-8755 (J.L.); Fax: +86-27-6877-8229 (J.L.).

Academic Editors: Guy J-P. Schumann, George Petropoulos, Richard Gloaguen and Prasad S. Thenkabail

Received: 19 December 2014 / Accepted: 15 April 2015 / Published: 20 April 2015

Abstract: China's largest freshwater lake, Poyang Lake, is characterized by rapid changes in its inundation area and hydrodynamics, so in this study, a hydrodynamic model of Poyang Lake was established to simulate these long-term changes. Inundation information was extracted from Moderate Resolution Imaging Spectroradiometer (MODIS) remote sensing data and used to calibrate the wetting and drying parameter by assessing the accuracy of the simulated inundation area and its boundary. The bottom friction parameter was calibrated using current velocity measurements from Acoustic Doppler Current Profilers (ADCP). The results show the model is capable of predicting the inundation area dynamic through cross-validation with remotely sensed inundation data, and can reproduce the seasonal dynamics of the water level, and water discharge through a comparison with hydrological data. Based on the model results, the characteristics of the current velocities of the lake in the wet season and the dry season of the lake were explored, and the potential effect of the current dynamic on water quality patterns was discussed. The model is a

promising basic tool for prediction and management of the water resource and water quality of Poyang Lake.

Keywords: inundation area; remote sensing; hydrodynamic model; Poyang Lake; current velocity

1. Introduction

As important ecosystems and valuable surface water resources, lakes are under considerable threat from intensive human activities and dramatic climate change [1], which can result in water quality deterioration and water area shrink. China's largest freshwater lake, Poyang Lake, is also affected by these impacts [2]. Located in the north of Jiangxi Province and connected with the middle reach of the Yangtze River (Figure 1), Poyang Lake (28°22′–29°45′N and 115°47′–116°45′E) is a very important natural freshwater resource and ecological system in southeast of China that plays a crucial role in flood regulation and biodiversity protection [3]. In recent decades, many environmental problems have been occurring, including urban sewage inputs and non-point source pollutions from the watershed, which have led to the eutrophication of the lake water [4]. Moreover, the discharge of river sediment and sand dredging by humans have resulted in highly turbid lake water, which can harm aquatic organisms and influence the ecological balance of the lake [5]. Additionally, floods and droughts are becoming more and more frequent, and these can cause great destruction to the ecological environment and disrupt peoples' normal lives [6].

Hydrodynamics is a fundamental factor to sediment transport, and the dispersion of both phytoplankton and nutrients in the water which influences the biogeochemical systems of lakes [7]. Therefore, it is necessary to know the hydrodynamics patterns to better track and better understand sediment transport and algal blooms, which affect water quality. The water level of Poyang Lake can be less than 8 m in the dry season and more than 21 m in the wet season depending on watershed discharge and the water level of the Yangtze River [8]. Therefore, inundation and hydrodynamic patterns exhibits rapid and complicated dynamic patterns; the water surface area of the lake expands to approximately 3000 km^2 in the wet season and shrinks to less than 1000 km^2 in the dry season [9]. During the high water period, the lake is calm and the flow velocity is relatively low, but the flow velocity increases as the waters recede into the narrow river channels during low water periods [10].

For large lakes, flow measurements obtained from hydrographic surveys, which are limited in their temporal and spatial scales and resolution, are not sufficient to determine hydrodynamic patterns. However, the results of hydrodynamic models can be scaled to the desired spatial and temporal resolution of an entire study area [11,12]. Many studies have shown that there is significant value in performing comprehensive hydrodynamic simulations of lakes and reservoirs around the world to evaluate possible pollutant concentration levels and protect and manage water resources [7,13–15]. Given the importance of understanding Poyang Lake's hydrodynamic patterns, it is urgent that a reliable hydrodynamic model be established as a basis for the effective study of the water quality of the lake.

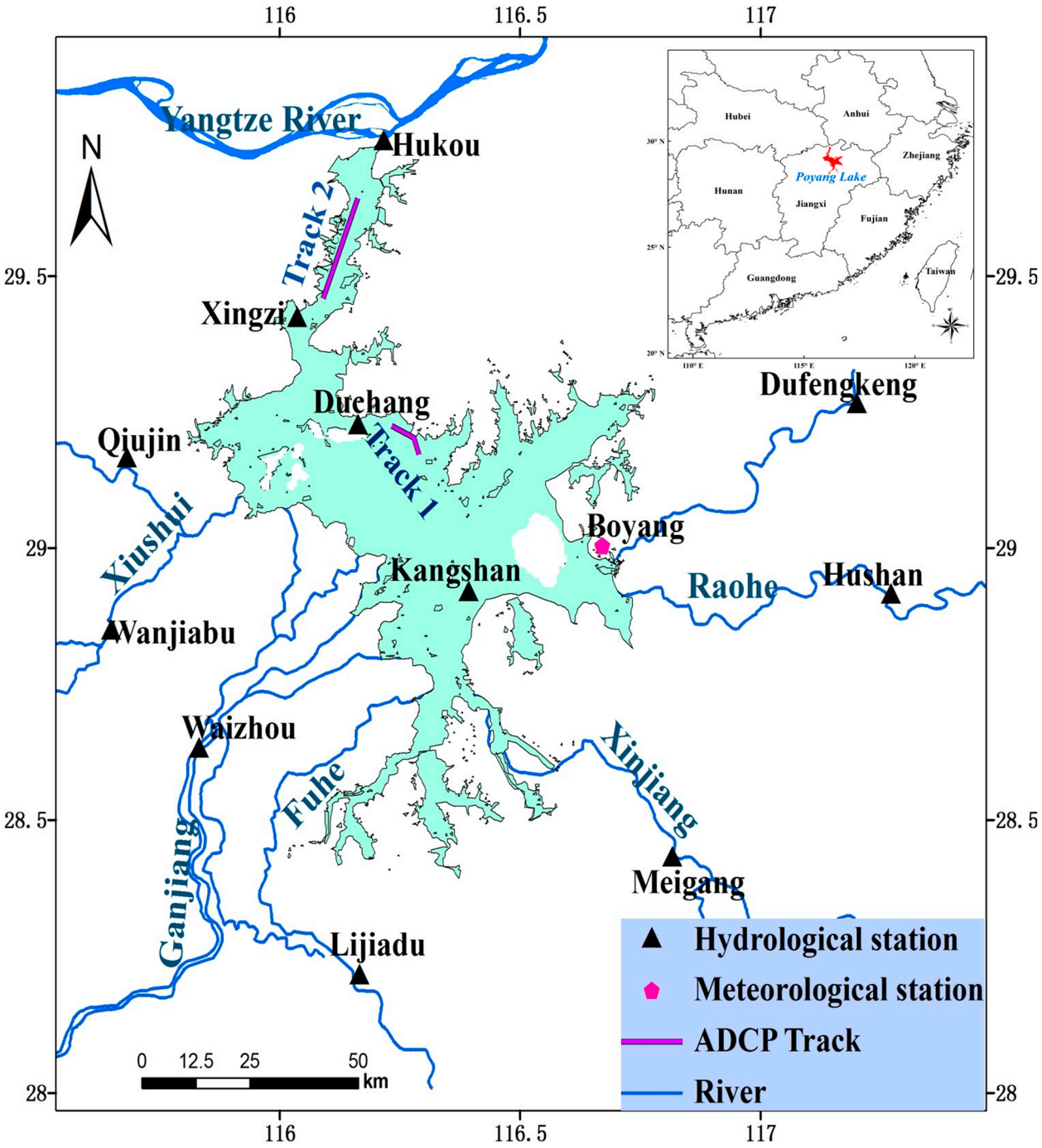

Figure 1. Study area and measurement sites.

Previous attempts to simulate the hydrodynamics of Poyang Lake have been limited. A coupled 1-D and 2-D model has been created to simulate the interaction between the Yangtze River and its linked lakes, including Poyang Lake [16]. However, the model is not concentrated on the hydrodynamics of Poyang Lake and the simulated current velocities were not calibrated and validated by field measurements. An integrated hydrological and hydrodynamic model has been established to simulate the water level change of Poyang Lake [17], but the wetting and drying process was not well represented in the model given the lake's rapid changes in inundation, and the model's ability to simulate the inundation has not been fully examined. Additionally, the above hydrodynamic models of Poyang Lake both ignore the accuracy of the modeled change in inundation area when simulating the

current velocity. As the lake inundation area expands or shrinks, some bathmetry are introduced into or deleted from the model, which synchronously influence flow conditions [18]. Therefore, the inundation process must be reasonably simulated to establish a reliable hydrodynamic model. In this study, inundation information extracted from remote sensing images was explored for calibration and validation to achieve a satisfactory inundation modeling of Poyang Lake.

This paper proposes an approach for accurate prediction of inundation area and hydrodynamics for the Poyang Lake, which is characterized by rapid changes in its inundation and hydrodynamics. The proposed approach is a combination of hydrodynamic model and remotely sensed data which is considered powerful and innovative. The established model is used to better reveal the hydrodynamic characteristics of the lake in this study. The paper is organized as follows. Section 2 describes the Poyang Lake study area and the data employed in this study, and the hydrodynamic model is described and model calibration process is described in Section 3. In Section 4, the ability of the model to simulate hydrodynamics and the dynamics of inundation area is analyzed through model calibration and validation results, and the spatial distribution characteristics of current velocity are analyzed and discussed. Conclusions are presented in the last section.

2. Study Area and Available Data

2.1. Study Area

The drainage basin of Poyang Lake has an area of 162,225 km^2 and five main rivers flows into the lake: the Xuishui, Ganjiang, Fuhe, Xinjiang, and Raohe (Figure 1). The water level of the lake is mainly controlled by catchment discharges and the interaction with the Yangtze River at the northern end of the lake. There is considerable seasonal variability in the water level of the lake, with a difference of approximately 13 m in the water height between the wet and dry seasons, which results in an obvious expansion and contraction of the lake area. The lake has a storage capacity of 27.6 billion m^3 and an average water depth of 8.4 m. The lake is geographically divided into two parts by Songmen Mountain: the southern lake is large and shallow, while the northern portion is a narrow and deep waterway [9]. The level of the lake bed decreases from approximately 18 m in the southern lake to approximately 1 m in the northern lake.

2.2. Data Preparation

Four types of data were used in this study. These included water level and water discharge data from hydrological stations, wind field datasets from one meteorological station, current velocity measured by Acoustic Doppler Current Profilers (ADCP) and remote sensing data from MODIS/Terra and MODIS/Aqua sensors between 2001 and 2010.

Daily water level and water discharge data from 2000–2011 were obtained from hydrological stations in Poyang Lake, although water level data were not available from the hydrological stations in in the year 2011. Water level data were collected from four stations: Xingzi, Duchang, Tangyin, and Longkou (Figure 1). The Poyang Lake basin consists of five river tributaries and five main rivers, which flow into the lake as described above. Water discharge data were collected from hydrological stations in the five rivers (Figure 1), and of these hydrological stations, Wanjiabu measures the

discharge for the Xiushui, Waizhou for the Ganjiang, Lijiadu for the Fuhe, Meigang for the Xinjiang, and Hushan and Dufengkeng for the Raohe. Water level and water flux records were collected at Hukou station, which is located at the junction of Poyang Lake and the Yangtze River, were collected (Figure 1). Daily wind field data were collected from Boyang (Figure 1), the nearest metrological station to Poyang Lake, from 2001–2011.

One cruise survey was conducted in July 2011, for which a small fishing boat was used. The current velocities were measured by the isochronous ship-board ADCP (Acoustic Doppler Current Profilers) in two tracks, which were both in the deep waterway and near to the lake shore (Figure 1). The first track was near Duchang hydrological station, and the current velocities were measured on 19 July 2011. The second track was in the southern lake (the waterway) in which the current velocities were measured on July 20, 2011. The distance between the ADCP measurement points along the tracks was about 50 m.

The MODIS Level-0 data (raw digital counts) collected between 2001 and 2010 were obtained from the NASA Goddard Space Flight Center (GSFC) [19]. Each Level-0 image consists of data collected from 36 spectral bands covering approximately 2330 km from east–west along the north–south satellite track. The spatial resolutions of these bands are approximately 250 m for bands 1~2, 500 for bands 3~7, and 1000 m for bands 8~36. Out of all of the images covering the study region between January 2001 and December 2010, 592 cloud-free images were selected for analysis. On some days, two cloud-free images were provided, one by the MODIS/Terra sensor in the morning and another by the MODIS/Aqua sensor in the afternoon. Table 1 lists the temporal distribution of the selected data, and there is at least one cloud-free image for any given month, and most months have at least two images. These high-frequency measurements ensure that the variability of the inundation area can be captured and used for the calibration of the hydrodynamic model in this study.

Table 1. Number of cloud-free MODIS images of Poyang Lake from 2001 to 2010.

Month	2001	2002	2003	2004	2005	2006	2007	2008	2009	2010
Jan	2	5	6	2	2	6	8	6	9	3
Feb	1	1	4	5	1	1	8	6	4	3
Mar	2	1	3	5	3	2	3	6	4	5
Apr	1	2	3	5	7	3	3	4	8	2
May	3	2	4	3	1	3	6	5	9	8
Jun	1	1	1	2	6	1	1	1	1	1
Jul	5	9	6	4	2	2	2	2	4	3
Aug	1	3	4	3	1	3	3	2	5	9
Sep	5	5	7	7	8	9	7	5	5	4
Oct	4	11	14	12	10	4	8	4	11	9
Nov	7	5	9	10	5	6	13	15	10	11
Dec	2	1	7	12	12	10	3	9	4	4
Total	34	46	68	70	58	50	65	65	74	62

3. Methods

Figure 2 shows a flow chart of the methodologies used in this study. The flowchart comprises four main phases: (1) Extraction of inundation area from satellite images; (2) Establishment of the hydrodynamic model; (3) parameters calibration for inundation and hydrodynamic modeling; and (4) model evaluation

with measurements and remotely sensed inundation area. Based on the model-predicted results, the characteristics of current velocity of Poyang Lake were finally analyzed. Each phase is detailed in the subsequent sections.

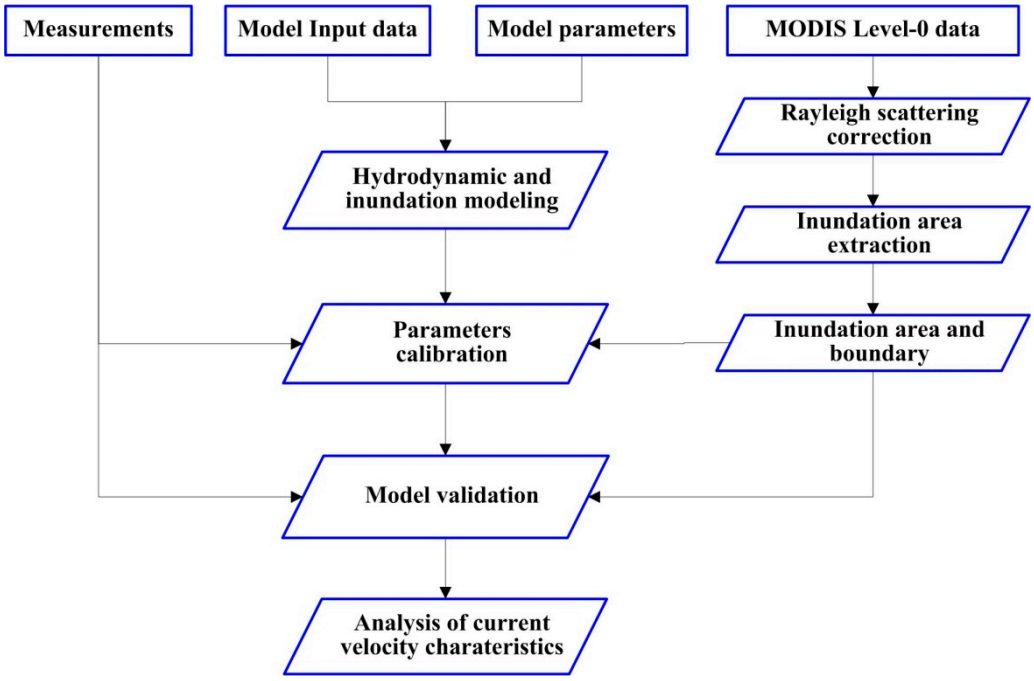

Figure 2. Flow chart of the methodologies.

3.1. Extraction of the Inundation Area

In this study, the FAI (Floating Algae Index), that originally designed by Hu (2009) [20] to detect floating algae in global oceans and inland waters, was used to extract water area of Poyang Lake [9]. FAI has been successfully used to delineated the water/land boundary of Taihu Lake of China [21]. It has been demonstrated that FAI is not sensitive to variable solar/viewing geometry and aerosol type and thickness, and the MODIS global surface reflectance products (MOD09GQ and MYD09GQ with sinusoidal projection) available at the USGS LPDAAC could not be used to derive FAI by Hu (2009). So the MODIS Level-0 data were collected and only Rayleigh scattering was corrected to derive the reflectance.

The selected MODIS Level-0 data were processed using the SeaDAS software (version 6.4) provided by NASA [22]. After correction for Rayleigh scattering and the effects of gaseous absorption, the Rayleigh-corrected reflectance (R_{rc}) data were georeferenced into a cylindrical equidistance (rectangular) projection. $R_{rc,\lambda}$ was derived as follows [20]:

$$R_{rc,\lambda} = \pi L^*_{t,\lambda} / (F_{0,\lambda} \times cos\theta_0) - R_{r,\lambda} \quad (1)$$

where λ is the wavelength of the MODIS spectral band, L^*_t is the calibrated sensor radiance after correction for gaseous absorption, F_0 is the extraterrestrial solar irradiance, θ_0 is the solar zenith angle, and $R_{r,\lambda}$ is the reflectance due to Rayleigh scattering, which was estimated using the 6S radiative transfer code [23].

The FAI was derived from Rayleigh-corrected reflectance data as follows:

$$\mathrm{FAI} = R_{\mathrm{rc},859} - R'_{\mathrm{rc},859} \tag{2}$$

$$R'_{rc,859} = R_{rc,645} + (R_{rc,1240} - R_{rc,645}) \times (859 - 645)/(1240 - 645) \tag{3}$$

where the numbers denote the MODIS wavelengths in nanometers. The 500-m resolution band at 1240 nm was resampled to 250 m to match the resolution at the 645-nm and 859-nm bands. FAI is essentially $R_{rc,859}$, where the inclusion of the two neighboring bands ($R'_{rc,859}$) provides a simple atmospheric correction. More detailed theory about FAI and the derivation process can be found in Hu (2009) [20].

FAI values over water are much lower than over land, suggesting that a potential FAI threshold value may be derived to separate the two. A gradient method proposed by Feng (2012) [9] was used to determine the water/land interface and the corresponding FAI threshold. For each FAI image a gradient image was derived, in which a pixel's gradient was determined by its neighboring 3 × 3 pixel window:

$$\mathrm{gradient} = \sqrt{\frac{1}{8}\sum_{i=1}^{8}\left(\frac{dy_i}{dx_i}\right)^2} \tag{4}$$

where dy_i and dx_i denote the changes in the FAI value and pixel location for each of the adjacent 8 pixels. Due to the strong water absorption at the near infrared region, FAI shows a strong gradient over the water/land pixels. The maximum gradient values near the water/land interface can be considered as the threshold for water/land delineation. Based on the gradient method, the inundation boundary of the lake was extracted and the inundation area was determined by summing all of the pixels classified as water.

3.2. Establishment of the Poyang Lake Hydrodynamic Model

In this study, the Delft3D-FLOW numerical modeling system, which has been widely applied in two-dimensional hydrodynamic simulations of lakes [24–29], is used to set up the two-dimensional hydrodynamic model of Poyang Lake. This system has been developed for the modeling of unsteady water flow, temperature, salinity and cohesive/non-cohesive sediment transport in shallows seas, estuarine and coastal areas, rivers and lakes [30]. Delft3D-FLOW solves the shallow water equations for a given set of initial and boundary conditions in two or three dimensions. The continuity and the horizontal momentum equations are solved by an implicit finite difference method (ADI) on a staggered (spherical or orthogonal curvilinear) grid. Delft3D-FLOW solves the Navier Stokes equations for an incompressible fluid under the shallow water and Boussinesq assumptions. In the orthogonal curvilinear coordinate (ξ, η) systems, a depth-averaged two-dimensional flow continuity equation and momentum equations can be described as follows:

Continuity equation:

$$\frac{\partial \varsigma}{\partial t} + \frac{1}{\sqrt{G_{\xi\xi}G_{\eta\eta}}}\frac{\partial[(d+\varsigma)u\sqrt{G_{\eta\eta}}]}{\partial \xi} + \frac{1}{\sqrt{G_{\xi\xi}G_{\eta\eta}}}\frac{\partial[(d+\varsigma)u\sqrt{G_{\xi\xi}}]}{\partial \eta} = 0 \tag{5}$$

Momentum equations:

$$\begin{aligned}&\frac{\partial u}{\partial t} + \frac{u}{\sqrt{G_{\xi\xi}}}\frac{\partial u}{\partial \xi} + \frac{v}{\sqrt{G_{\xi\xi}}}\frac{\partial v}{\partial \eta} + \frac{uv}{\sqrt{G_{\xi\xi}G_{\eta\eta}}}\frac{\partial \sqrt{G_{\xi\xi}}}{\partial \eta} - \frac{v^2}{\sqrt{G_{\xi\xi}G_{\eta\eta}}}\frac{\partial \sqrt{G_{\eta\eta}}}{\partial \xi} - fv \\ &= -\frac{P_\xi}{\rho\sqrt{G_{\xi\xi}}} - gu\frac{\sqrt{u^2+v^2}}{c^2(d+\xi)} + F_\xi\end{aligned} \tag{6}$$

$$\frac{\partial v}{\partial t}+\frac{u}{\sqrt{G_{\xi\xi}}}\frac{\partial v}{\partial \eta}+\frac{v}{\sqrt{G_{\xi\xi}}}\frac{\partial u}{\partial \xi}+\frac{uv}{\sqrt{G_{\xi\xi}G_{\eta\eta}}}\frac{\partial\sqrt{G_{\xi\xi}}}{\partial \eta}-\frac{u^2}{\sqrt{G_{\xi\xi}G_{\eta\eta}}}\frac{\partial\sqrt{G_{\eta\eta}}}{\partial \xi}+fu$$
$$=-\frac{P_\eta}{\rho\sqrt{G_{\xi\xi}}}-gv\frac{\sqrt{u^2+v^2}}{c^2(d+\xi)}+F_\eta \quad (7)$$

where ς is the free surface elevation above the reference plane, d is the water depth below the reference plane; $\sqrt{G_{\xi\xi}}$ and $\sqrt{G_{\eta\eta}}$ are the coefficients used to transform curvilinear to rectangular coordinates in the ξ direction and the η direction, respectively; u and v represent the depth-averaged velocity in the ξ direction and the η direction, respectively; P_ξ and P_η represent the pressure gradients in the ξ direction and the η direction, respectively; and F_ξ and F_η represent the turbulent momentum flux in the ξ direction and the η direction, respectively. Finally, f is the Coriolis coefficient, and ρ is the density of water.

Before setting up the model, the boundary of the model area must be determined, and because the time range for the model in this study is from 2001–2011, the maximum inundation area in this time span was selected from the remote sensing images (Table 1). The maximum inundation area calculated from the remote sensing images was captured in August 2010 during a quadrennial flood process [31]. However, the calculated inundation area consists of some nearby small lakes and conservation areas separated by dikes, and the water in these isolated areas does not interact with the water in Poyang Lake. Therefore, based on the maximum inundation area from the remote sensing image, the model area was determined by deleting the isolated areas. The water boundary was then obtained through digitization in a GIS system (Figure 3).

Orthogonal curvilinear model grids were generated under the Cartesian coordinate system based on the water boundary. To better capture the rapid dynamic of inundation area and minimize the computing effort, and also to facilitate the calibration and validation of the simulated inundation area and boundary, the size of the generated model grids varied from 200–300 m, which was close to the spatial resolution of the inundation images (250 m). The bathmetry at each computational node of the model grids (Figure 3) is interpolated from the bathmetry data measured by the Changjiang Water Resources Commission of China [32]. Model run time extended from January 1, 2001 to December 31, 2011, and the model time step was set as 30 s in order to meet the Courant-Friedrich-Levy (CFL) criteria for a stable solution [33]. Daily wind data from Boyang metrological station were used as the spatial-uniform driving force for the water surface. The lower open boundary condition was set at the junction between the lake and the Yangtze River at Hukou. In this lake model based on Delft3D, the open boundary type was time-series water levels and the daily water levels measured at Hukou station were prescribed at the grid points along the open boundary. The river flow rates measured at the hydrological stations along the five main five rivers were prescribed as the upper inflow boundary condition of the river inlets (Figure 1). Velocity condition at the lower open boundary and the upper inflow boundary was not prescribed in this two dimensional lake model because the depth-averaged velocity was calculated based on momentum equation (Delft3D User Manual, 2011). The water level was initialized as the mean of the measured water level from the four hydrological stations (Xingzi, Duchang, Tangying, and Longkou) in Poyang Lake on January 1, 2001, and the current velocities were initialized with zero values. Consequently, the current velocities in the lake from the upper river mouth to the open boundary were calculated in this hydrodynamic model.

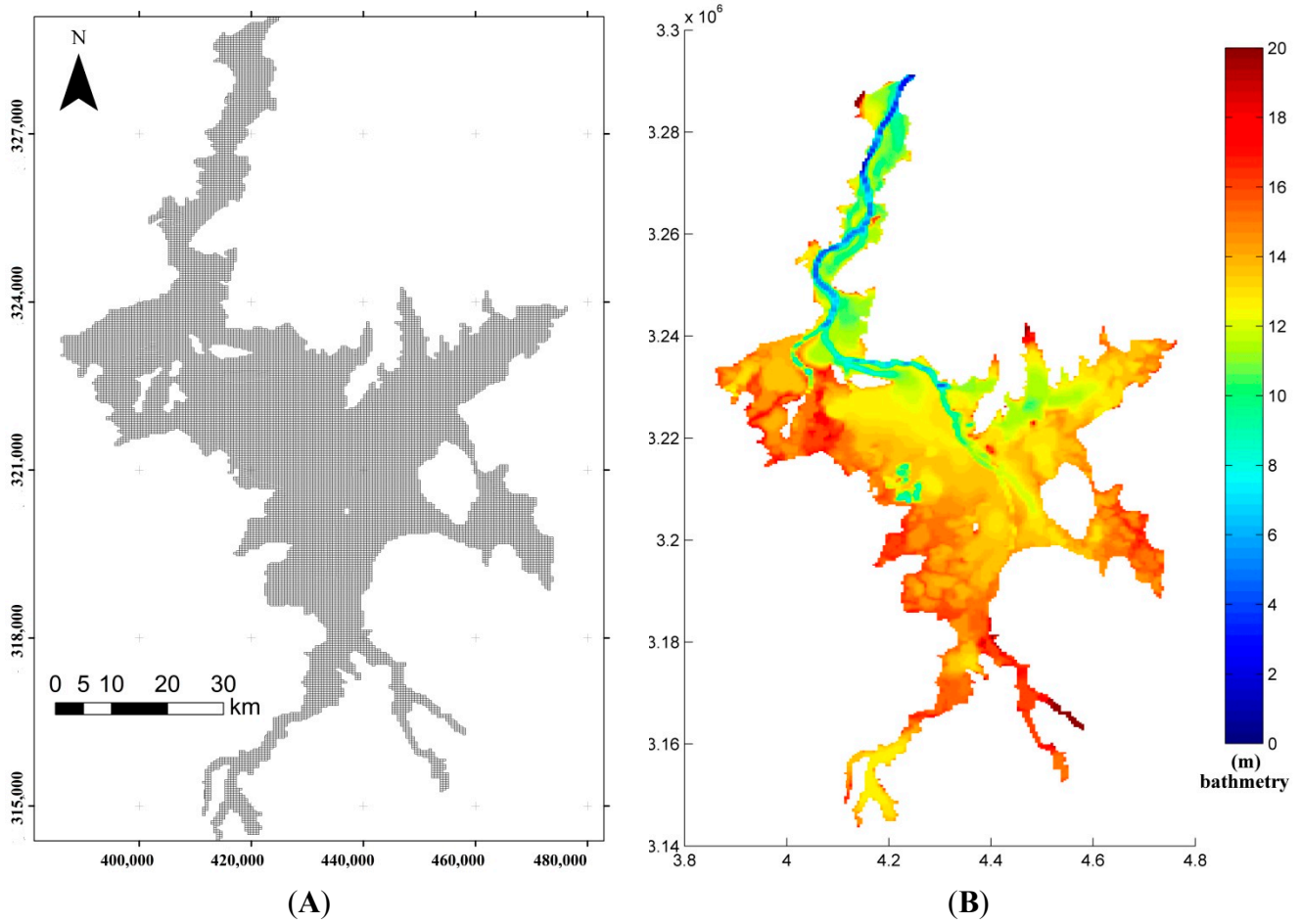

Figure 3. Model grids (**A**) and bathmetry (**B**).

3.3. Model Parameter Calibration

In this study, the main parameters of the two-dimensional hydrodynamic model of Poyang Lake were the Manning roughness coefficient, the eddy viscosity parameter and the critical water depth for wetting and drying; the trial-and-error method was used to calibrate these parameters. The Manning roughness and eddy viscosity parameters were manually adjusted by repeat modeling to achieve a consistent simulated result with the field measured velocities from the ADCP and water levels and water discharges from the hydrological stations.

Our model calibration focused on reproducing the inundation area dynamic of Poyang Lake because the rapid change in water inundation is the defining characteristic of the lake. With the recession and flooding of water, the model grids become wet and dry, and the wet grids make up the inundation area. The wetting and drying process, which is most commonly addressed in tidal circulation modeling [18], is also of concern in this lake model. The wetting and drying scheme in Delft3D-FLOW is typical of finite difference models in that a series of checks are performed to determine if a grid point is wet or dry based on the water depth relative to a threshold value specified by the user. If the water depth at a cell face drops below a specified critical water depth, the velocity across that face is set to zero, and no momentum or mass transfer occurs. This system, while simple, is robust and effective [18].

Therefore, in the inundation modeling of Poyang Lake, the critical water depth controlling the wetting and drying of the grids should be calibrated. In this study, both the inundation area and

inundation boundary extracted from the MODIS images were used to calibrate this parameter. The inundation area was used to calibrate this parameter through a comparison with the simulated inundation area by trial and error. Moreover, the Cohen's Kappa coefficient is used to evaluate the agreement between model-simulated and remotely sensed inundation boundaries.

Kappa is commonly used to assess accuracy by measuring the agreement between model predictions and reality [34], and it is a generic term for the measurement of agreement with categorical data. For example, Kappa is widely used to assess the accuracy of the classifications of remotely sensed data [34]. In this study, the remotely sensed and model-simulated inundation data were assigned to two categories, the inundated area and the non-inundated area. The Kappa measure of agreement is the following ratio:

$$K = \frac{P_A - P_E}{1 - P_E} \tag{8}$$

where K denotes the Kappa coefficient, P_A is the proportion of observed agreement, and P_E is the proportion of agreement expected by chance

$$\mathrm{P_A} = \frac{\mathrm{S}}{\mathrm{N}} \tag{9}$$

$$P_E = \frac{a_1 b_1 + a_0 b_0}{N^2} \tag{10}$$

where N is the total number of model grids, S is the total number of grids that are in both the inundation area and the non-inundation area in the remotely sensed data and model-simulated results, $a_1$and b_1 are the numbers of inundated grids in the remotely sensed data and model-simulated results, respectively, and a_0 and b_0 are the numbers of non-inundated grids in remotely sensed data and model-simulated results, respectively. It should be noted that the size of the model grids (200 m–300 m) is not the same as the size of the remote sensing pixel (250 m), but they are very close. Thus, in this study, the nearest neighbor sampling method is used to calculate the number of non-inundated grids, a_1, and the number of non-inundated grids, a_0, in the remotely sensed data. The resulting value of K ranges from −1~1 and complete agreement between the inundation boundaries corresponds to K = 1; a lack of agreement corresponds to K = 0 and K = 0.8~1 denotes very good agreement. Negative value of Kappa would indicate disagreement between inundation boundaries.

3.4. Model Evaluation

To conduct the trial-and-error calibration and model validation, some quantitative information is required to measure model performance through a comparison of the inundation area data from remotely sensed images and the hydrological data with the model results. The values of some statistical performance indices were calculated to evaluate the model performance: the root mean square error (RMSE), the goodness of fit (R^2), the Nash–Sutcliffe efficiency coefficient (NSE), the percentage of bias (PBIAS), the RMSE-observations standard deviation ratio (RSR). The RMSE (Equation (11)) indicates a perfect match between observed and predicted values when it equals 0 (zero), with increasing RMSE values indicating an increasingly poor match. The NSE (Equation (12)) ranges between −∞ and 1. It indicates a perfect match between observed and predicted values when NSE = 1. Values between 0.0 and 1.0 are generally viewed as acceptable levels of performance,

whereas values less than 0.0 indicate that the mean observed value is better than the simulated value, which indicates unacceptable performance. The coefficient R^2 (Equation (13)), which ranges between 0 and 1, describes the proportion of the variance in the measured data, which is explained by the model, with higher values indicating less error variance. The PBIAS (Equation (14)) measures the average tendency of the simulated data to be larger or smaller than their observed counterparts. The optimal value of PBIAS is 0.0, with low magnitude values indicating an accurate model simulation. Positive values indicate underestimation bias, and negative values indicate over-estimation bias. The RSR (Equation (15)) is calculated as the ratio of the RMSE and standard deviation of measured data. RSR varies from the optimal value of 0, to a large positive value with lower RSR values indicating better model performance.

$$\mathrm{RMSE} = \sqrt{\frac{\sum_{i=1}^{n}(P_i - O_i)^2}{n}} \tag{11}$$

$$\mathrm{NSE} = \frac{\sum_{i=1}^{n}(O_i - \bar{O})^2 - \sum_{i=1}^{n}(P_i - O_i)^2}{\sum_{i=1}^{n}(O_i - \bar{O})^2} \tag{12}$$

$$\mathrm{R}^2 = \frac{[\sum_{i=1}^{n}(O_i - \bar{O})(P_i - \bar{P})]^2}{\sum_{i=1}^{n}(O_i - \bar{O})^2 \sum_{i=1}^{n}(P_i - \bar{P})^2} \tag{13}$$

$$\mathrm{PBIAS} = \frac{\sum_{i=1}^{n}(O_i - P_i)}{\sum_{i=1}^{n}(O_i)} \times 100\% \tag{14}$$

$$\mathrm{RSR} = \frac{RMSE}{STDE_{obs}} = \sqrt{\frac{\sum_{i=1}^{n}(O_i - P_i)^2}{\sum_{i=1}^{n}(O_i - \bar{O}_i)^2}} \tag{15}$$

where n is the number of observations in the periods under consideration, O_i is the i-th observed value, $\bar{O}_i$ is the mean observed value, P_i is the i-th model simulated value, and $\bar{P}_i$ is the mean model simulated value.

4. Results and Discussion

4.1. Model Calibration and Validation Results

4.1.1. Inundation Modeling

In this study, the remotely sensed inundation data of Poyang Lake from 2001–2005 were used to calibrate the critical water depth for wetting and drying, and the remotely sensed inundation data of Poyang Lake from 2006–2010 were used to validate the inundation modeling. The calibration experiments were manually conducted by repeatedly refining the critical water depth for wetting and drying from 0.05–0.65 m, and the RMSE of the simulated inundation area was calculated for each calibration experiment. In addition, the Kappa coefficients for the maximum and minimum inundation area captured by the remote sensing in each year were calculated. Then, the mean Kappa coefficients for the maximum inundation area (MKMAX) and the mean Kappa coefficients for the minimum inundation area (MKMIN) were obtained for each calibration experiment. Figure 4 shows the variation of the RMSE, the MKMAX and the MKMIN. It is found, with the increase of the critical water depth,

the RMSE first decreased and then increased, and both the MKMAX and MKMIN first increased and then decreased. The minimum RMSE and the maximum MKMIN were achieved when the critical water depth was 0.45 m, but the maximum MKMAX was achieved when the critical water depth was 0.50 m. By balancing the simulated inundation area error and the inundation boundary agreement between model results and the remotely sensed data, the value of 0.45 m was determined to be the critical water depth for wetting and drying in the model to simulate the inundation area dynamic of Poyang Lake.

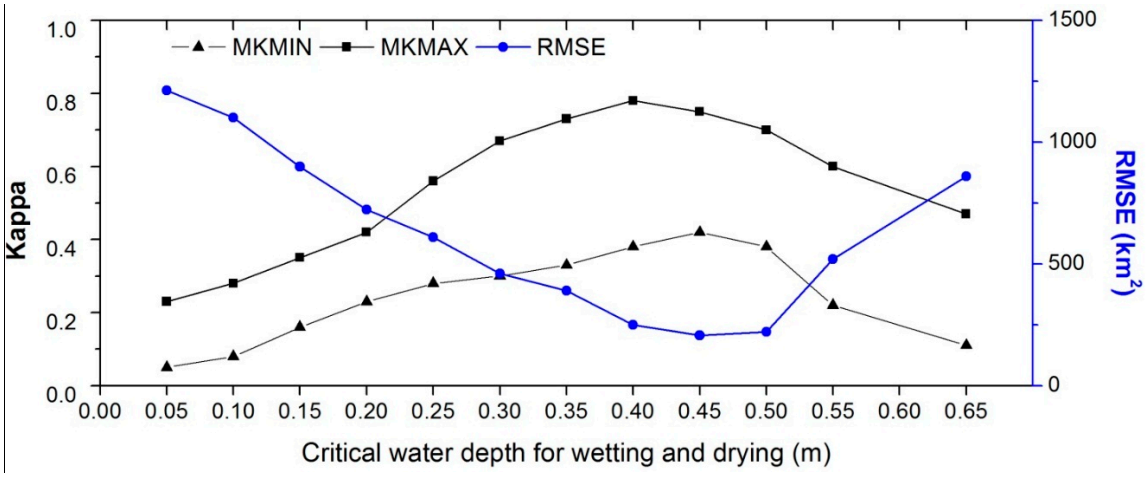

Figure 4. RMSE values of the simulated inundation areas, the mean Kappa coefficient for the maximum remotely sensed inundation area (MKMAX) and mean Kappa coefficient for the minimum remotely sensed inundation area (MKMIN) during the model calibration period (2001–2005) for calibration experiments with different critical water depth.

The simulated and remotely sensed inundation area extracted from the MODIS images are compared both in the calibration period (2001–2005) and the validation period (2006–2010) (Figure 5). It demonstrates that the simulated inundation areas are in satisfactory consistence with remote sensing data from 2001–2010. Table 2 displays the statistical indices for the simulated inundation areas in the calibration and the validation periods. The RMSE values of the simulated inundation in the calibration period and validation periods are 206.24 km^2 and 183.65 km^2, respectively. The Nash–Sutcliffe efficiency coefficient (NSE), the R^2, and the RMSE-observations standard deviation ratio (RSR) all show that the model have a good performance in inundation area modeling in the calibration and validation periods. The percentage of bias (PBIAS) reveals that the simulated inundation areas both in the calibration period and validation periods were slightly underestimated but reasonably acceptable. These results indicate that the critical water depth parameter for wetting and drying was well calibrated, and the model has the capability to predict the variations in the inundation of Poyang Lake under complex hydrodynamic changes.

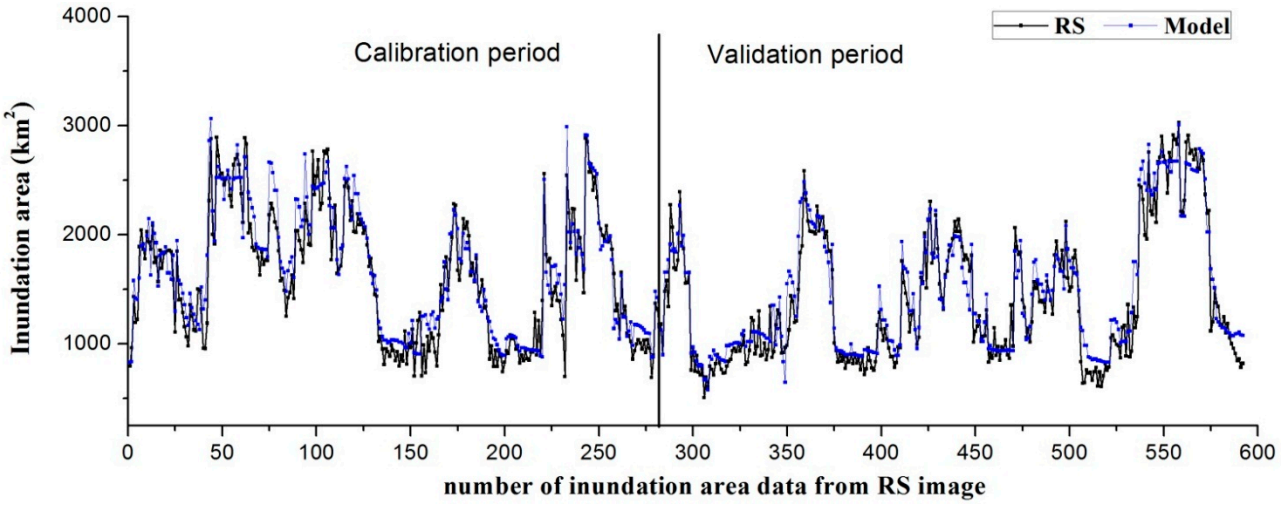

Figure 5. Comparison of simulated and remotely sensed inundation areas in the calibration period (2001–2005) and the validation period (2006–2010).

Table 2. Calibration and validation statistics for the simulations of inundation area, water level and water discharge.

	Statistical Index	Inundation Area	Water Level				Hukou Discharge
			Xingzi	Duchang	Tangyin	Longkou	
Calibration period	RMSE	206.2	0.32	0.59	0.42	0.25	530.6
	NSE	0.87	0.99	0.95	0.96	0.97	0.83
	R^2	0.90	0.99	0.97	0.96	0.98	0.89
	PBIAS	−0.04	0.002	0.02	0.01	0.002	0.15
	RSR	0.36	0.10	0.23	0.20	0.17	0.38
Validation period	RMSE	183.6	0.53	0.67	0.42	0.22	398.9
	NSE	0.91	0.98	0.95	0.95	0.97	0.90
	R^2	0.92	0.99	0.97	0.96	0.97	0.95
	PBIAS	−0.04	−0.02	−0.02	−0.01	−0.004	0.13
	RSR	0.30	0.15	0.22	0.21	0.18	0.27

The water boundary of the maximum and minimum inundation area captured by remote sensing and the corresponding simulated inundation boundary at the time of remotely sensed data acquisition are compared within the validation period (Figure 6). The comparisons show the simulated inundation boundaries satisfactorily match those extracted from remote sensing images. The MKMAX in the validation period is 0.83, revealing a good matching of the inundation boundary. The mismatching between the simulated and remotely sensed boundaries to different degrees over the minimum inundation area can be observed in the validation period, and the MKMIN is only 0.24. The disagreement between the simulated and remotely sensed lake area in the dry season, when the lake area is less than 1000 km^2, is also obvious (Figure 5). This outcome could probably be attributed to two aspects. First, the bathymetry is so complex that the model could not capture the inundation area with a relatively coarse model grid size when the total lake area is small and divided into a large number of small lakes. Second, the model grid size (200~300 m) and image resolution (250 m) do not exactly match each other, which results in the deviation during boundary matching.

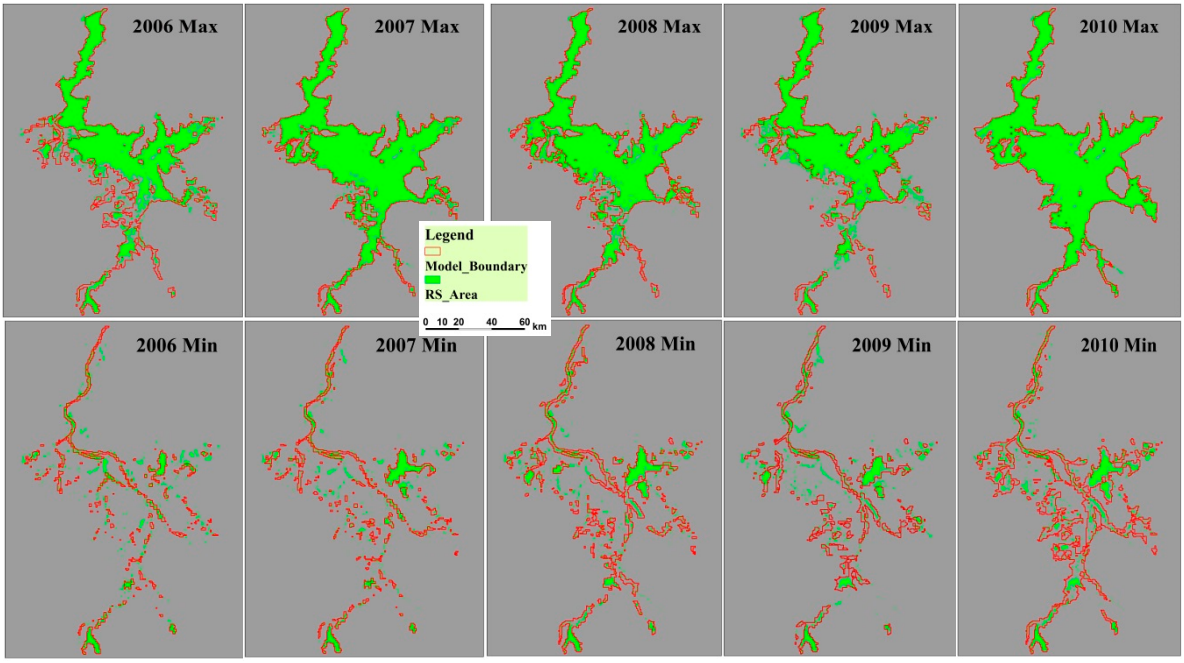

Figure 6. Model simulated water boundary (Model_Boundary) and remotely sensed inundation area (RS_Area) at the time of maximum (Max) and minimum (Min) inundation area for each year from 2006 to 2010.

Generally, the hydrodynamic model is capable of satisfactorily capturing the dynamic of Poyang Lake inundation area following calibration and validation by remote sensing data, which can captured the real state of nature. However, optical remote sensing sensor fails to capture the signal reflected by water when the weather is cloudy. Furthermore, the revisit cycle of a remote sensing satellite is generally several days, so remote sensing cannot capture the daily or even hourly state of the water inundation. The hydrodynamic model can fill in the gaps from remote sensing inundation monitoring because it is capable of continuously outputting the inundation data in small time steps. This is of great significance for Poyang Lake, which is characterized by dramatic changes in inundation. Consequently, the success of the model in predicting the inundation area dynamics makes it a promising tool for monitoring and managing changing water resources.

4.1.2. Hydrodynamic Modeling

The Manning roughness and eddy viscosity parameters were manually refined using a simple trial and error method. By comparing the simulated results with ADCP-measured current velocities, water levels and water discharge from hydrological stations, the optimal Manning roughness and eddy viscosity values were found to be 0.26 and 0.28, respectively, when good hydrodynamic modeling performance was achieved. Figure 7 shows that the simulated velocities are reasonably consistent with the measurements along the two ADCP tracks. For, The RMSEs of the simulated velocities on the two ADCP tracks were 0.028 m/s and 0.031 m/s, respectively, the NSE values were 0.91 and 0.88, respectively, the R^2 values were 0.91 and 0.89, respectively, and the RSR values were 0.29 and 0.34, respectively, all of which indicate satisfactory model performance. The PBIAS were −0.01 and −0.006 for the respective tracks, which represents a slight underestimation of the simulated velocities. This

could be due to measurement errors caused by nearby sailing vessels at some ADCP points, because the ADCP tracks were near the deep waterway.

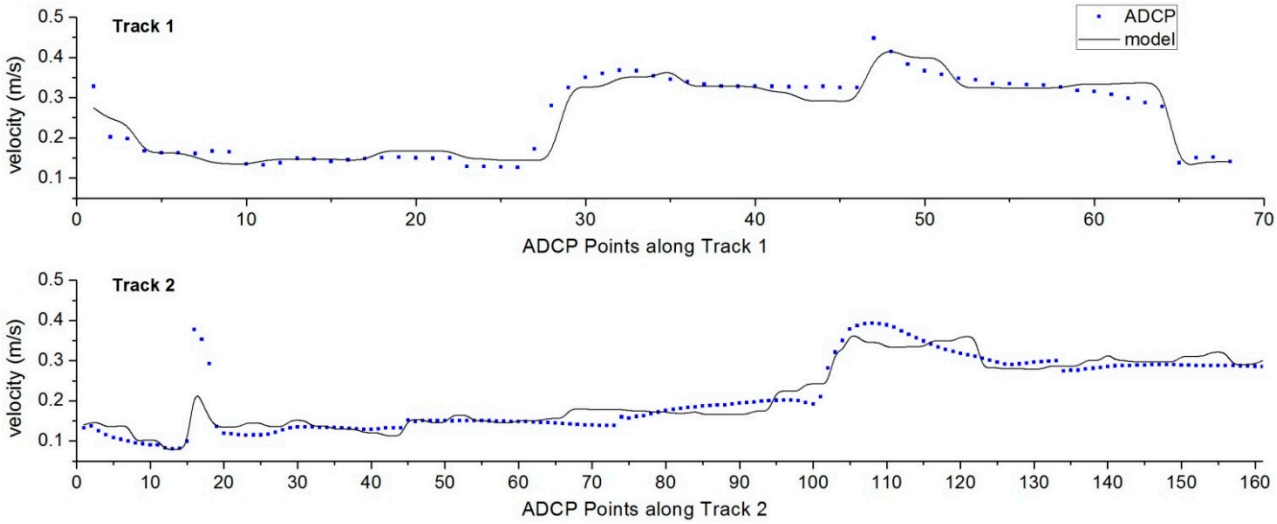

Figure 7. Comparison of simulated and measured velocities along two separated ADCP tracks.

Water levels from the model results and hydrological stations (Xingzi, Duchang, Tangyin, and Longkou) were compared in both the calibration period (2001–2005) and the validation period (2006–2010) (Figure 8), and the model results generally match the measured water levels and can reproduce the seasonal and annual water level dynamics. As shown in Table 2 for the statistical indices of the simulated water level at the hydrological stations during the calibration and calibration periods, the RMSE values range from 0.22 to 0.67 m; the RSR values range from 0.1 to 0.23; the NSE values are all above 0.95, and the R^2 values are all above 0.96, indicating satisfactory model calibration and validation. The PBIAS values show the simulated water level is slightly underestimated due to discrepancies between the simulated and gauged low lake water levels that occur during the dry season (October to March). This outcome probably arises from the complex lake bathymetry and the interactions between the wetlands and lake storage, which likely exert greater influence over the predictions of low than high water levels. A satisfactory consistency between the simulated water discharges from the lake into the Yangtze River results and the gauged discharge at Hukou station was achieved (Figure 8), which also show that the model can reasonably reproduce the backflow periods and the backflow flowrate. It shows that the backflow process took place in 2002, 2003, 2004, 2005, 2007, and 2008 to different degrees. Table 2 shows that the NES values of the simulated water discharge during the calibration and validation periods at Hukou are 0.83 and 0.90, respectively; the R^2 values are 0.89 and 0.95, respectively, and the RSR values are 0.38 and 0.27, respectively, all of which indicate satisfactory model performance. The statistical indices reveal that the calibrated parameters seem more appropriate for the water discharge modeling of the validation periods. Generally, the hydrodynamics of Poyang Lake can be well predicted by this effectively calibrated and validated model.

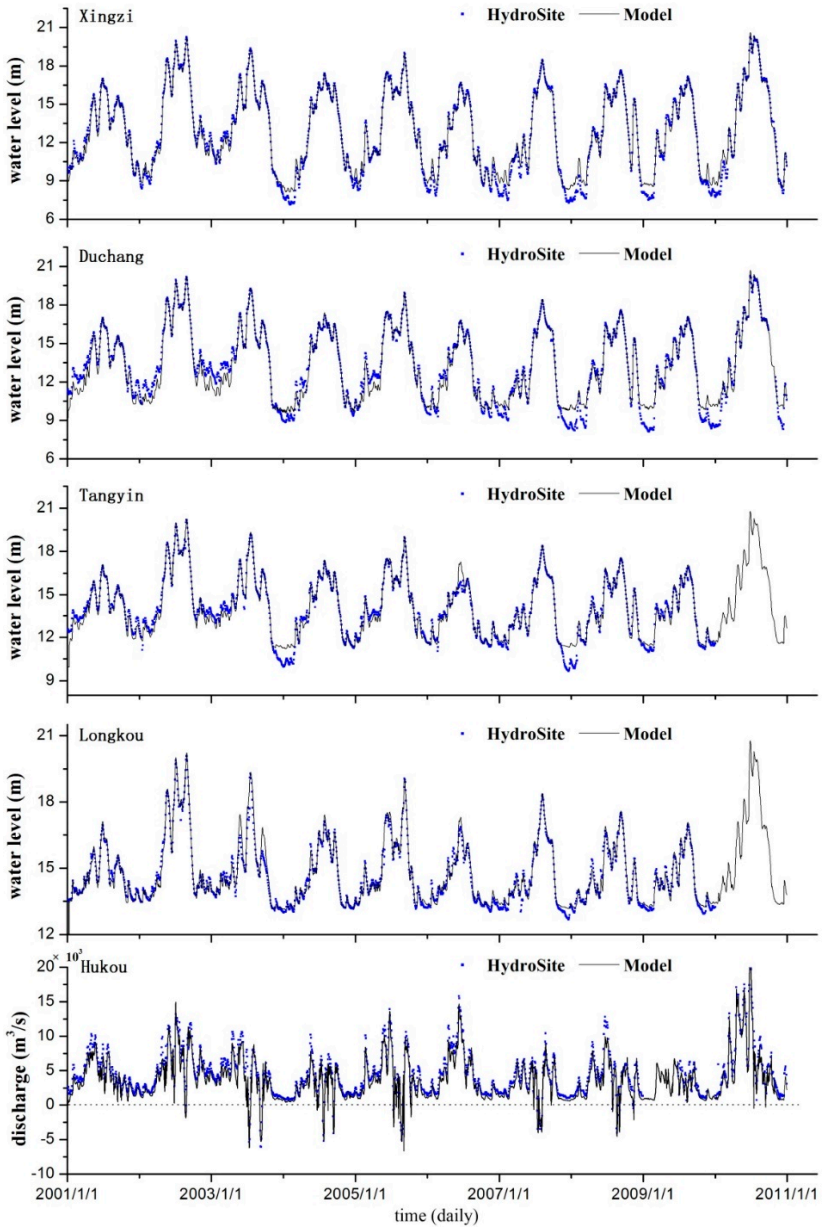

Figure 8. Comparison of water level and water discharge from the model and the hydrological stations during the calibration periods (2001–2005) and the validation periods (2006–2010). Note that the water level measurements at Tangyin and Longkou are not available in the year 2010.

4.2. The Current Velocity Characteristics

The water flows in Poyang Lake are characterized by gravity currents that are driven by runoff from the Poyang Lake watershed. As a consequence of the seasonal changes in the inflows from the five rivers, the hydrodynamics of the lake show highly temporal variations. In addition, the complex bathmetry and particular morphology of the lake could shape the special spatial distribution patterns of current velocity fields. Based on the results of the hydrodynamic model, the variable spatial pattern of the current flows of Poyang Lake are analyzed and discussed.

The spatial distributions of the monthly averaged current directions and current magnitudes in the dry season (November, 2005) and in the wet season (June, 2005) were plotted (Figure 9). It can be

observed that the waters flow from the river mouth into the lake, and then flood into the narrow waterway in the northern part of the lake with increased current velocities in both the wet and dry season (Figure 9A,B). This shows that the directions of the currents throughout the lake were hardly altered despite the rapid seasonal changes in the inundation area.

On the whole, the magnitude of the current velocity in the dry season is greater than that in the wet season (Figure 9C,D) because the difference in the water level between the southern lake and the northern lake in the dry season is greater than in the wet season. This can be observed by comparing the water levels at the four hydrological stations (Figure 8). In the wet season, the current magnitude in the northern lake is clearly greater than in the southern lake (Figure 9D). However, in the dry season as the water recedes into the narrow and deep waterway, the current velocity in the main part of the northern lake increases (Figure 9C), and the difference in the current velocities between the northern lake and the southern lake is reduced.

The current velocities in the narrow and deep waterway of the northern lake are above 0.25 m/s in both the wet season and the dry season and are significantly higher than those in the nearby shallow water area of the northern lake (Figure 9C,D). Waters in this area flow along the waterway and flow directions are mostly to the northeast. The current velocities in the main part of the southern lake are generally between 0.05 m/s and 0.25 m/s, and waters flow from the river mouth into this area and then rush into the northern lake from the narrow passage near Duchang. In the southern lake, there are many bays on the edge of the lake, including the northeastern bay and other small bays near the river mouths. The current velocities in these lake bays are much smaller, mostly less than 0.05 m/s and smaller than those in the main part of the southern lake. Waters in these bays are relatively close together with less water exchange with waters in the main part of the lake, especially during the dry season. Put simply, the overall current velocity in Poyang Lake reveals significant spatial variability.

According to the current velocity characteristics of Poyang Lake, the lake can be roughly classified as consisting of three parts: (1) the northern lake; (2) the main part of the southern lake; and (3) the lake bays on the edge of the lake. Current velocities in the first part are distinctly higher than in the other two parts, and the current velocities in the third part are lower than in the other two parts. This classification is roughly the same as that used in previous studies [35,36] that divided the lake into these three parts based on hydro-geomorphology. These studies found that the relative water residence times in the three parts, from short to long, were as follows: the northern lake, the main part of the southern lake, and the bays on the edge of the lake. Considering the current velocity characteristics of the three parts, it could reveal that the lake area with higher current velocities would have a longer water residence time. Because residence time dominates the transport and fate of the pollutants in the waters, the current velocities in the lake should be an important indicator of water quality. Studies have shown that total phosphorus, total nitrogen and chlorophyll-a concentrations in the lake bays are higher than those in the rest of the lake [35]. From this point of view, the results of the hydrodynamic model could be beneficial for the assessment of the water quality of Poyang Lake. Moreover, the water quality management of Poyang Lake should consider the different hydrodynamic conditions affected by the dynamics of the inundation area. To quantitatively calculate the residence time in the different parts of the lake, the Lagrangian model could be used in further studies.

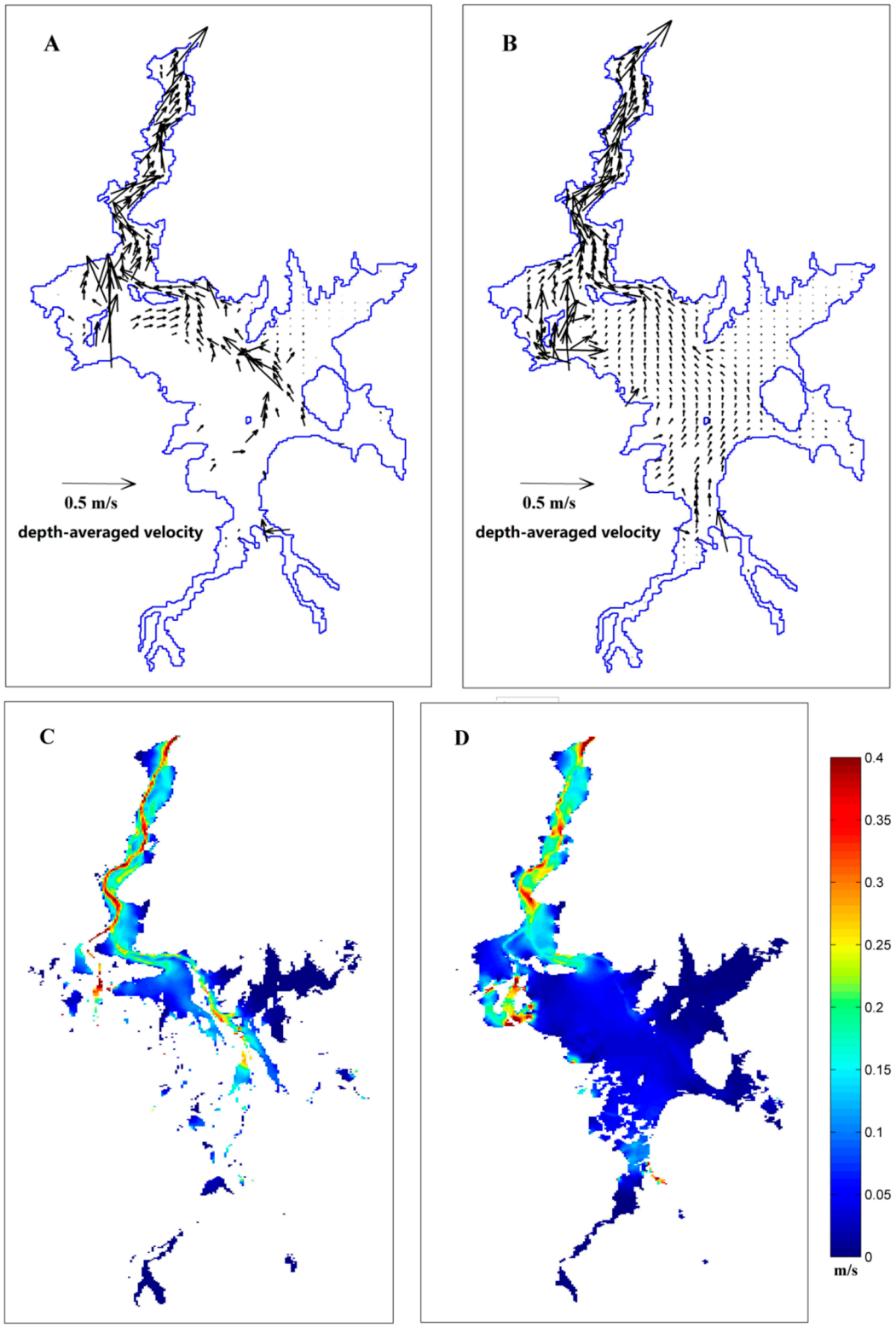

Figure 9. Monthly mean depth-averaged current vectors and magnitudes in the dry season (June, 2005) and the wet season (November, 2005). (**A**) and (**B**) are current vectors in the dry season and wet season, respectively, and (**C**) and (**D**) are current magnitudes in the dry season and wet season, respectively.

5. Conclusions

A hydrodynamic and inundation model of Poyang Lake, China's largest freshwater lake, was developed, and the inundation information extracted from MODIS images was explored to calibrated and validate the model and enhance its ability to simulate the dynamic of inundation area. The inundation data were then used as the input or background data for the hydrodynamic model, which was calibrated with *in situ* current velocity and hydrological data. Based on the hydrodynamic model, the spatial distribution characteristics of current velocity were analyzed and the potential effects on water quality were explored.

The model is a promising tool to monitor the inundation area dynamics of Poyang Lake, which will be of benefit to water resource management. Because hydrodynamics play a crucial role in the transport and fate of contaminants, the model will be useful for water quality assessment when dealing with the dramatic dynamics of inundation areas.

This study shows the potential in integrating remotely sensed inundation data with hydrodynamic models to predict the dynamic of water inundation areas. Further research can use cloud removal methods of optical satellite images to generate more cloud-free images [37], which will benefit the hydrodynamic model development and inundation area prediction. Future work could build the sediment transport and biochemical models based on this hydrodynamic model, which will be useful for predicting geomorphic and ecological effect from climate variability and anthropogenic activities.

Acknowledgments

This work was supported by the National Natural Science Foundation of China (Grant Nos. 41331174, 41101415, 41401388, 51179109), the National Key Technology R&D Program (Grant No. 2012BAC06B04), and the Collaborative Innovation Center for Major Ecological Security Issues of Jiangxi Province and Monitoring Implementation (Grant No. JXS-EW-08). We are thankful for the Delft Hydraulics for providing the open source code of Delft3D-FLOW. The constructive comments from three anonymous reviewers are greatly appreciated.

Author Contributions

Peng Zhang conducted model calibration and validation and prepared the manuscript draft; Jianzhong Lu established the hydrodynamic model; Lian Feng processed MODIS data and together with Xiaoling Chen helped to outline the manuscript structure; Li Zhang, Xiongwu Xiao and Honggao Liu prepared and pre-processed the field and satellite data. All authors read and approved the final manuscript.

Conflicts of Interest

The authors declare no conflict of interest.

References

1. Jones, R.; McMahon, T.; Bowler, J. Modelling historical lake levels and recent climate change at three closed lakes, Western Victoria, Australia (c. 1840–1990). *J. Hydrol.* **2001**, *246*, 159–180.

2. Ye, X.; Zhang, Q.; Liu, J.; Li, X.; Xu, C. Distinguishing the relative impacts of climate change and human activities on variation of streamflow in the Poyang Lake catchment, China. *J. Hydrol.* **2013**, *494*, 83–95.
3. Ye, X.; Zhang, Q.; Bai, L.; Hu, Q. A modeling study of catchment discharge to Poyang Lake under future climate in China. *Quatern. Int.* **2011**, *244*, 221–229.
4. Chen, X.; Zhang, Y.; Zhang, L.; Chen, L.; Lu, J. Distribution characteristic of nitrogen and phosphorus in Poyang Lake during high water periods. *J. Lake Sci.* **2013**, *25*, 643–648.
5. Feng, L.; Hu, C.; Chen, X.; Tian, L.; Chen, L. Human induced turbidity changes in Poyang Lake between 2000 and 2010: Observations from MODIS. *J. Geophys. Res.: Oceans* **2012**, *117*, doi:10.1029/2011JC007864.
6. Yin, H.; Li, C. Human impact on floods and flood disasters on the Yangtze River. *Geomorphology* **2001**, *41*, 105–109.
7. León, L.F.; Imberger, J.; Smith, R.E.; Hecky, R.E.; Lam, D.C.; Schertzer, W.M. Modeling as a tool for nutrient management in lake erie: A hydrodynamics study. *J. Great Lakes Res.* **2005**, *31*, 309–318.
8. Lai, X; Huang, Q; Zhang, Y; Jiang, J. Impact of lake inflow and the yangtze river flow alterations on water levels in Poyang Lake, China. *Lake Reserv. Manage.* **2014**, *30*, 321–330.
9. Feng, L.; Hu, C.; Chen, X.; Cai, X.; Tian, L.; Gan, W. Assessment of inundation changes of Poyang Lake using modis observations between 2000 and 2010. *Remote Sens. Environ.* **2012**, *121*, 80–92.
10. Cheng, S.; Ru, B. The characteristics of the lake current of Poyang Lake. *Jiangxi Hydraul. Sci. Technol.* **2003**, *29*, 105–108.
11. Zhang, Z.; Beletsky, D.; Schwab, D.J.; Stein, M.L. Assimilation of current measurements into a circulation model of lake michigan. *Water Resour. Res.* **2007**, *43*, doi:10.1029/2006WR005818.
12. Stroud, J.R.; Lesht, B.M.; Schwab, D.J.; Beletsky, D.; Stein, M.L. Assimilation of satellite images into a sediment transport model of Lake Michigan. *Water Resour. Res.* **2009**, *45*, doi:10.1029/2007WR006747.
13. Hurdowar-Castro, D.; Tsanis, I.; Simanovskis, I. Application of a three-dimensional wind driven circulation model to assess the locations of new drinking water intakes in Lake Ontario. *J. Great Lakes Res.* **2007**, *33*, 232–252.
14. Preston, A.; Hannoun, I.A.; List, E.J.; Rackley, I.; Tietjen, T. Three-dimensional management model for Lake Mead, Nevada, Part 1: Model calibration and validation. *Lake Reserv. Manage.* **2014**, *30*, 285–302.
15. Preston, A.; Hannoun, I.A.; List, E.J.; Rackley, I.; Tietjen, T. Three-dimensional management model for Lake Mead, Nevada, Part 2: Findings and applications. *Lake Reserv. Manage.* **2014**, *30*, 303–319.
16. Lai, X.; Jiang, J.; Liang, Q.; Huang, Q. Large-scale hydrodynamic modeling of the middle Yangtze River basin with complex river–lake interactions. *J. Hydrol.* **2013**, *492*, 228–243.
17. Li, Y.; Zhang, Q.; Yao, J.; Werner, A.; Li, X. Hydrodynamic and hydrological modeling of the Poyang Lake catchment system in China. *J. Hydrol. Eng.* **2013**, *19*, 607–616.
18. Medeiros, S.C.; Hagen, S.C. Review of wetting and drying algorithms for numerical tidal flow models. *Int. J. Numer. Methods Fluids* **2013**, *71*, 473–487.

19. Modis web. Available online: http://modis.gsfc.nasa.gov/ (accessed on 20 April 2015).
20. Hu, C. A novel ocean color index to detect floating algae in the global oceans. *Remote Sens. Environ.* **2009**, *113*, 2118–2129.
21. Hu, C.; Lee, Z.; Ma, R.; Yu, K.; Li, D.; Shang, S. Moderate resolution imaging spectroradiometer (MODIS) observations of cyanobacteria blooms in Taihu Lake, China. *J. Geophys. Res.: Oceans* **2010**, *115*, doi:10.1029/2009jc005511.
22. Ocean color sedas. Available online: http://seadas.Gsfc.Nasa.Gov/installers/ (accessed on 20 April 2015).
23. Vermote, E.F.; Tanré, D.; Deuze, J.-L.; Herman, M.; Morcette, J.-J. Second simulation of the satellite signal in the solar spectrum, 6s: An overview. *IEEE Trans. Geosci. Remote Sens.* **1997**, *35*, 675–686.
24. Razmi, A.M.; Barry, D.A.; Bakhtyar, R.; le Dantec, N.; Dastgheib, A.; Lemmin, U.; Wüest, A. Current variability in a wide and open lacustrine embayment in lake geneva (Switzerland). *J. Great Lakes Res.* **2013**, *39*, 455–465.
25. Kuang, C.; He, L.; Xing, F.; Deng, L.; Gu, J. Numerical study on the evolution process of polluted water cluster in gonghu, taihu lake. In Proceedings of the 3rd International Conference on Bioinformatics and Biomedical Engineering, 2009 (ICBBE 2009), Beijing, China, 11–13 June 2009; pp. 1–4.
26. El-Adawy, A.; Negm, A.; Elzeir, M.; Saavedra, O.; El-Shinnawy, I.; Nadaoka, K. Modeling the hydrodynamics and salinity of El-Burullus Lake (Nile Delta, noRthern Egypt). *J. Clean Energy Technol.* **2013**, *1*, doi:10.7763/JOCET.2013.V1.37.
27. Razmi, A.M.; Barry, D.A.; Lemmin, U.; Bonvin, F.; Kohn, T.; Bakhtyar, R. Direct effects of dominant winds on residence and travel times in the wide and open lacustrine embayment: Vidy Bay (Lake Geneva, Switzerland). *Aquat. Sci.* **2014**, *76*, 59–71.
28. Kaçıkoç, M.; Beyhan, M. Hydrodynamic and water quality modeling of Lake Eğirdir. *Clean Soil Air Water* **2014**, *42*, 1573–1582.
29. Xing, F.; Kettner, A.; Syvitski, J.; Ye, Q.; Bevington, A.; Twilley, R.; Atkinson, J. Impact of Vegetation on the Hydrodynamics and Morphological Changes of the Wax Lake Delta during Hurricane*s*. In Proceedings of American Geophysical Union Fall Meeting, San Francisco, CA, USA, 9–13 December 2013.
30. Lesser, G.; Roelvink, J.; van Kester, J.; Stelling, G. Development and validation of a three-dimensional morphological model. *Coast. Eng.* **2004**, *51*, 883–915.
31. Jiangxi hydrology. Available online: http://www.Jxsw.Cn/item/6811.Aspx (accessed on 20 April 2015, in Chinese).
32. Changjiang water resources commission of china. Available online: http://www.cjw.gov.cn/ (accessed on 20 April 2015, in Chinese).
33. Hydraulics, D. *Delft3D-Flow, Simulation of Multi-Dimensional Hydrodynamic Flows and Transport Phenomena, Including Sediments*; User Manual; Deltares: Rotterdamseweg, The Netherlands, 2006
34. Congalton, R.G. A review of assessing the accuracy of classifications of remotely sensed data. *Remote Sens. Environ.* **1991**, *37*, 35–46.

35. Zhang, L.; Chen, X.; Zhang, Y.; Chen, L.; Zhang, P. Spatial distribution of water quality and its impacting factor in the wet season of Poyang Lake using the hydro-geomorphological partitions. *China Environ. Sci.* **2014**, *34*, 2637–2645.
36. Hu, C. The Water Environmental Charateristics and Its Evolutionary Trends of Poyang Lake. Ph.D. Thesis, Nanchang University, Nanchang, China, 2010.
37. Li, Y.; He, R. Spatial and temporal variability of sst and ocean color in the gulf of maine based on cloud-free SST and chlorophyll reconstructions in 2003–2012. *Remote Sens. Environ.* **2014**, *144*, 98–108.

© 2015 by the authors; licensee MDPI, Basel, Switzerland. This article is an open access article distributed under the terms and conditions of the Creative Commons Attribution license (http://creativecommons.org/licenses/by/4.0/).